

Rotating self-gravitating Bose-Einstein condensates with a crust: a minimal model for pulsar glitches

Akhilesh Kumar Verma,^{1,*} Rahul Pandit,^{1,†} and Marc E. Brachet^{2,‡}

¹*Centre for Condensed Matter Theory, Department of Physics,
Indian Institute of Science, Bangalore 560012, India.*

²*Laboratoire de Physique de l'École Normale Supérieure, ENS, Université PSL,
CNRS, Sorbonne Université Université de Paris, 24 Rue Lhomond, 75005 Paris, France*

(Dated: May 28, 2020)

We develop a minimal model for *pulsar glitches* by introducing a solid-crust potential in the three-dimensional (3D) Gross-Pitaevskii-Poisson equation (GPPE), which we have used earlier to study gravitationally bound Bose-Einstein Condensates (BECs), i.e., bosonic stars. In the absence of the crust potential, we show that, if we rotate such a bosonic star, it is threaded by vortices. We then show, via extensive direct numerical simulations (DNSs), that the interaction of these vortices with the crust potential yields (a) stick-slip dynamics and (b) dynamical glitches. We demonstrate that, if enough momentum is transferred to the crust from the bosonic star, then the vortices are expelled from the star, and the crust's angular momentum J_c exhibits features that can be interpreted naturally as glitches. From the time series of J_c , we compute the cumulative probability distribution functions (CPDFs) of event sizes, event durations, and waiting times. We show that these CPDFs have signatures of self-organized criticality (SOC), which have been seen in observations on pulsar glitches.

Rotating magnetized neutron stars [1, 2], or *pulsars*, display *glitches*, which are sudden increases of their rotational frequencies. These observations have a long history [3–5]; and they indicate that glitches are associated with the transfer of angular momentum, which is carried by quantum vortices in the superfluid interior, to the solid crust, in the outer layers of the pulsar. This transfer occurs because of vortex-crust interactions, as suggested in Refs. [6, 7]. The quantitative modeling of pulsar glitches is complex, so different models have been suggested [1, 8]: some involve avalanches of superfluid vortices [9]; other mainstream models are based on neutron superfluidity in the crust [10].

Neutron Cooper pairs [11], which comprise a major component of the nuclear matter in a pulsar, form a superfluid. Therefore, Refs. [12, 13] have proposed simply to model this superfluid by using the two-dimensional (2D) Gross-Pitaevskii equation (GPE); in addition, they have included an externally imposed potential or *container* and a *pinning* potential for the crust. However, pulsars are three dimensional (3D); and gravitational effects are important on stellar scales. It is important, therefore, to account for these crucial features in a model for pulsars and the glitches they exhibit. In this Letter, we construct a *natural, minimal model* for pulsar glitches by (a) accounting for gravitational effects via the Gross-Pitaevskii-Poisson equation (GPPE) for a self-gravitating superfluid (see, e.g., Refs. [4, 14, 15] for a non-rotating bosonic star) and (b) including *rotation* and an *interacting* solid crust.

We carry out extensive pseudospectral direct numerical simulations (DNSs) to show that our minimal model yields pulsar glitches with properties that are akin to those seen in observations. In particular, the time se-

ries of the angular momentum J_c of the crust shows the hallmarks of self-organized criticality (SOC) [17–24]. To obtain these results, we develop a sophisticated algorithm to find the ground state of the GPPE, with rotation: this algorithm uses an ancillary advective real Ginzburg-Landau-Poisson equation (ARGLPE), an imaginary-time version of the GPPE. The resulting ground states *contain vortices* and yield uniformly rotating solutions of the GPPE. When we include the crust and its dynamics, we find a transfer of the angular momentum from the star to the crust, where it is dissipated by friction; if this transfer is large enough, vortices move outwards and glitches are observed.

Self-gravitating GPPE superfluids are described by a complex wave function $\psi(\mathbf{x}, t)$, governed by the following partial differential equation (PDE):

$$i\hbar\partial_t\psi = -\frac{\hbar^2}{2m}\nabla^2\psi + [V_\theta + G\Phi + g|\psi|^2]\psi; \quad (1)$$

$$\nabla^2\Phi = |\psi|^2 - \langle |\psi|^2 \rangle; \quad (2)$$

here, m is the mass of the bosons, $n = |\psi|^2$ their number density, $G = 4\pi G_N m^2$ (G_N denotes Newton's gravitational constant), and $g = 4\pi a\hbar^2/m$, with a the s -wave scattering length [38]. We describe the dynamics of the pulsar's solid crust by a single polar angle θ , which evolves as follows:

$$I_c \frac{d^2\theta}{dt^2} = \frac{1}{N} \int d^3x \partial_\theta V_\theta |\psi|^2 - \alpha \frac{d\theta}{dt}; \quad (3)$$

$$V_\theta(\mathbf{r}_p) = V_0 \exp\left(-\frac{|\mathbf{r}_p| - r_{\text{crust}}}{\Delta r_{\text{crust}}}\right)^2 \tilde{V}(x_\theta, y_\theta); \quad (4)$$

I_c and V_θ denote, respectively, the moment of inertia of the crust and the crust potential; α controls the frictional slowing down of the rotation of the crust, with

$\sqrt{I_c/\alpha}$ the crust-friction decay time; for specificity, we choose $\tilde{V}(x_\theta, y_\theta) = 3 + \cos(n_{\text{crust}}x_\theta) + \cos(n_{\text{crust}}y_\theta)$, with $x_\theta = \cos(\theta)x_p + \sin(\theta)y_p$ and $y_\theta = -\sin(\theta)x_p + \cos(\theta)y_p$; here, n_{crust} determines the number of pinning sites in the crust potential, r_{crust} is the radius at which this potential is a maximum, and Δr_{crust} determine the thickness of the crust. We use periodic boundary conditions (PBCs), so, to obtain a periodic version of the angular momentum J_z of the GPPE condensate, we use the π -centered, 2π -periodic coordinates: $\mathbf{r}_p = (x_p, y_p, z_p)$, with $x_p = -\sum_1^{10} \exp(-\frac{16}{100}n^2)(-1)^n \frac{\sin(n(x-\pi))}{n}$, $y_p = -\sum_1^{10} \exp(-\frac{16}{100}n^2)(-1)^n \frac{\sin(n(y-\pi))}{n}$, and $z_p = \pi$ (x_p and y_p are nearly linear near the center because they are truncated Fourier expansions of saw-tooth waves).

The crust *acts* on the GPPE superfluid *and also reacts* to it [39]. If $\alpha = 0$, the GPPE-crust coupled system (3) and (5) (or the Lagrangian from which it is derived) obeys the following global conservation laws: (a) Rotational invariance, *in the whole space* \mathbb{R}^3 , which leads to the conservation of the total angular momentum $J = J_c + J_z$, with $J_c = I_c \frac{d\theta}{dt}$ the crust angular momentum and $J_z = \int d^3x \bar{\psi}(\hat{\mathbf{e}}_z \times \mathbf{r}) \cdot (-i\hbar\nabla)\psi$. (b) Time-translation invariance, by virtue of which the total energy $E_{\text{tot}} = E + E_c$ is also conserved; here, $E_c = \frac{1}{2}(\frac{d\theta}{dt})^2$ is the rotational energy of the crust and E is the energy of the GPPE system, which we rewrite as

$$i\hbar \frac{\partial \psi}{\partial t} = -\frac{\hbar^2}{2m} \nabla^2 \psi + [V_\theta + (G\nabla^{-2} + g)|\psi|^2]\psi. \quad (5)$$

Equation (5) conserves the number of particles $N = \int d^3x |\psi|^2$ and (for time-independent θ) the GPPE energy $E = E_{kq} + E_{\text{int}} + E_G + E_V$, where $E_{kq} = \frac{\hbar^2}{2m} \int d^3x |\nabla\psi|^2$, $E_{\text{int}} = \frac{g}{2} \int d^3x (|\psi|^2)^2$, $E_G = \frac{G}{2} \int d^3x (|\psi|^2) \nabla^{-2} (|\psi|^2)$ and $E_V = \int d^3x |\psi|^2 V_\theta$. For $V_\theta = 0$, the momentum $\mathbf{P} = \frac{i\hbar}{2} \int d^3x (\psi \nabla \bar{\psi} - \bar{\psi} \nabla \psi)$ is also conserved.

We solve the GPPE 5 by using a 3D Fourier pseudospectral method [1–3], with $\psi(x) = \sum_{|\mathbf{k}| < k_{\text{max}}} \hat{\psi}_{\mathbf{k}} \exp(i\mathbf{k} \cdot \mathbf{x})$ and $k_{\text{max}} = [\mathcal{N}/3]$, where \mathcal{N} is the resolution and $[\cdot]$ denotes the integer part. In the absence of the crust potential, friction, and of rotation, we obtain the conventional GPPE [see Ref. [4], where we discuss the gravitational Jeans instability and the pseudospectral method (see also the Supplemental Material [28])]. In all 3 spatial directions, our DNS uses 2π -periodic PBCs, which we also use for J_z and V_θ ; so, even if $\alpha = 0$, the conservation of the total angular momentum holds only approximately, for the system does not have rotational invariance in \mathbb{R}^3 .

We first obtain uniformly rotating states for the GPPE with rotational speed Ω by solving the imaginary-time equation

$$\hbar \partial_t \psi = -\frac{\delta}{\delta \bar{\psi}} (E - \Omega J_z - \mu N - \lambda (\frac{\mathbf{P}}{N_0 m})^2). \quad (6)$$

Rotational ground states are minima of $E - \Omega J_z$; μ , the

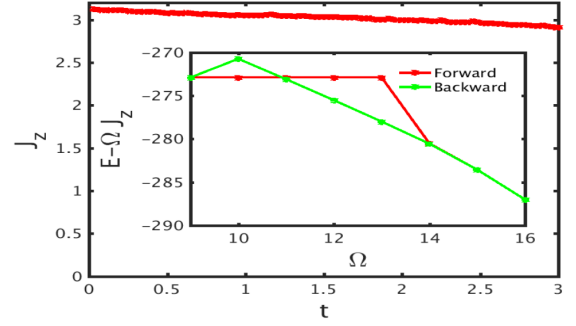


FIG. 1: Illustrative plot of the GPPE condensate angular momentum J_z vs time t ; J_z is not conserved exactly (decay of $\simeq 1\%$ per turn) because rotational symmetry holds only approximately if we use PBCs. Parameters: $\mathcal{N} = 64$, $g = 5$, $G = 50$, and $\Omega = 14$; the system has 4 vortices. Inset: Plot of the ARGLPE-converged value (see text) of $E - \Omega J_z$ vs the rotation speed Ω ; the differences between scans with increasing (red) and decreasing (green) Ω indicate hysteresis; the system has no vortices along the horizontal part of the red line and 4 vortices along the green one.

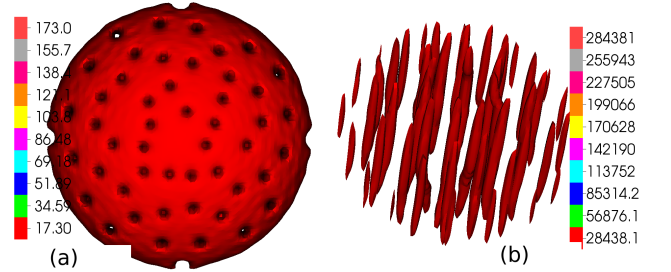


FIG. 2: Isosurface plots illustrating a rotating, compact object with vortices obtained via the ARGLPE (see text): (a) Isosurfaces of the boson density (top view); for the spatiotemporal evolution of these isosurfaces see the video S1 in the Supplemental Material [28]; and (b) isosurfaces of $(\nabla \times (\rho \mathbf{v}))^2$ (side view); here, $\mathcal{N} = 256$, $G = 800$, $g = 80$, and $\Omega = 60$.

chemical potential, and λ are Lagrange multipliers; at each time step, we tune μ to keep the boson number fixed; and we choose a large value of λ so that \mathbf{P} is small. We now obtain the following advective real Ginzburg-Landau equation (ARGLPE):

$$\hbar \frac{\partial \psi}{\partial t} = \frac{\hbar^2}{2m} \nabla^2 \psi + \mu \psi - [V_\theta + (G\nabla^{-2} + g)|\psi|^2]\psi - i\hbar(\Omega \hat{\mathbf{e}}_z \times \mathbf{r}_p - \lambda \frac{\mathbf{P}}{N_0 m}) \cdot \nabla \psi, \quad (7)$$

which we solve to obtain the rotational ground states (minima) mentioned above; to stabilise this minimization procedure, we reset the center of mass $\mathbf{r}_{\text{cm}} = \int d^3x \mathbf{r}_p |\psi|^2 / N$ to $(\pi, \pi, 0)$, after each time step.

We obtain rotational ($\Omega \neq 0$) states by integrating Eq. (7) until we get convergence; given our initial data, the system contains N bosons. For $\Omega = 0$ and $V_\theta = 0$, the

solution of the ARGLPE (7) converges, at large times, to ground states ψ_0 that are spherically symmetric, compact objects of radius R . This radius can be estimated by using a variational ansatz [29] or it can be computed numerically at both zero temperature ($T = 0$) [14, 15] and finite temperature ($T > 0$) [4]. We start from the $T = 0$ state of Ref. [4]; and then we increase the value of Ω in steps of 1; at each such increase in the value of Ω , we use the converged ARGLPE state, from the previous value of Ω , as the initial data. In the inset of Fig. 1 we plot the ARGLPE-converged values of $E - \Omega J_z$ versus Ω ; from this plot it is apparent that the non-rotating state, with no vortices, loses its stability around $\Omega \simeq 14$, to a state with 4 vortices. We show scans in which Ω increases (red lines) and decreases (green lines). The differences between these scans indicate that this system exhibits hysteresis: It has no vortices along the horizontal part of the red line and 4 vortices along the green ones; and it goes from the 4-vortex branch back to the 0-vortex branch at $\Omega \simeq 9$. In Fig. 1 we give an illustrative plot of J_z versus time t for the GPPE evolution of the 4-vortex state at $\Omega = 14$; we see that J_z is not conserved perfectly, but it decreases slightly ($\simeq 1\%$ per turn). J_z is not conserved exactly because rotational symmetry holds only approximately, given our PBCs; the closer we are to the center of our computational domain the better is this rotational symmetry. We show, in Figs. 2(a) and (b), respectively, isosurface plots of the boson density (top view) and of $(\nabla \times (\rho v))^2$ (side view) for the converged solution of ARGLPE, with $\mathcal{N} = 256$, $G = 800$, $g = 80$, and $\Omega = 60$. Clearly, our ARGLPE-based algorithm yields rotating, self-gravitating Bose-Einstein condensates (BECs), with vortices in the GPPE; this has not been possible hitherto [40].

We turn now to the GPPE (5) coupled with the crust-rotation equation (3). In Figs. 3 (a)-(d), we plot the crust-potential isosurface in blue, with $V_\theta = 450$, and ten-level isosurfaces of $(\nabla \times (\rho v))^2$ for a representative set of parameters and the times (a) $t = 0.06$, (b) $t = 6.48$, (c) $t = 7.38$, and (d) $t = 9.72$. *On average*, the crust gains angular momentum from the superfluid, hence, at long times, these vortices move outwards after losing enough angular momentum to the crust (compare Figs. 3 (a) and (d)). However, the time series of the condensate and crust angular momenta, J_z and J_c , respectively, are complicated, and, as we show below, they display the signatures of SOC [17–24]. We illustrate this temporal evolution in Fig. 4, for the representative parameter values $V_0 = 180$, $n_{\text{crust}} = 12$, $I_c = 0.01$, $r_{\text{crust}} = 1.0$, $\Delta r_{\text{crust}} = 0.15$, $\Omega_0 = 14$, and $\alpha = 0.007$. In Fig. 4(a) we plot, versus the scaled time $t\Omega_0$, $(J_c/J_{c_0} - 14)$ [blue curve], J_z/J_{c_0} [red curve], and $(J_c + J_z)/J_{c_0}$ [green curve], where J_{c_0} is the initial angular momentum of the crust. This figure shows that, if we neglect the overall, gentle decay of the total angular momentum [41], fluctuations of J_c compensate for those in J_z . In Figs. 4(b) and (c)

we show expanded plots of J_c/J_{c_0} for $0 < t\Omega_0 \lesssim 170$ and $80 \leq t\Omega_0 \leq 100$, respectively, to illustrate the irregular nature of the time series of the angular momentum of the crust.

From the time series $J_c(t)$ (Figs. 4(a)-(c)), we see that the crust can lose (gain) angular momentum to (from) the superfluid, because vortices stick to (slip from) the crust. To characterize the statistical properties of these stick-slip events, we calculate the gain ΔJ_c in the crust angular momentum, between successive minima and maxima of $J_c(t)$; we call ΔJ_c the event size; we scale it by J_{c_0} . In Fig. 5(a) we present a log-log (base 10) plot of the cumulative probability distribution function (CPDF) $Q(\Delta J_c/J_{c_0})$; this yields the power-law behavior $Q(\Delta J_c/J_{c_0}) \sim (\Delta J_c/J_{c_0})^\beta$, for the part of the CPDF that lies in the region shaded gray; thus, the probability distribution function (PDF) $P(\Delta J_c/J_{c_0}) \sim (\Delta J_c/J_{c_0})^{\beta-1}$; by fitting the CPDF in the gray region, we find $\beta \simeq 0.7$.

Next, we calculate the event-duration time t_{ed} , i.e., the time difference between successive minima and maxima of $J_c(t)$, and thence the CPDF $Q(t_{\text{ed}}\Omega_0)$ (log-log, base 10, plot in Fig. 5(b)). This plot shows, in the shaded gray region, that $Q(t_{\text{ed}}\Omega_0) \sim (t_{\text{ed}}\Omega_0)^\gamma$, with $\gamma \simeq 2.1$. Clearly, the PDF $P(t_{\text{ed}}\Omega_0) \sim (t_{\text{ed}}\Omega_0)^{\gamma-1}$, in this region.

Finally, we compute the CPDF $Q(t_{\text{wt}}\Omega_0)$ of the waiting time t_{wt} , i.e., the time difference between two successive maxima. From the shaded gray region in the semi-log (base 10) plot in Fig. 5(c), we observe the exponential form $Q(t_{\text{wt}}\Omega_0) \sim \exp(-t_{\text{wt}}\Omega_0)$.

These power-law behaviors of $Q(\Delta J_c)$ and $Q(t_{\text{ed}})$ and the exponential tail of $Q(t_{\text{wt}})$ together show that the stick-slip motion, between superfluid vortices and the crust, yields the time series $J_c(t)$, which has all the signatures of SOC found in measurements of pulsar glitches [21–24]. Some classes of pulsars exhibit a glitch-size PDF of the type we have obtained in our model; in particular, they show a power-law behavior in this PDF, over a certain range of sizes; and the power-law exponents lie in the range $-0.13 \lesssim -(\beta - 1) \lesssim 2.4$. For the pulsar PSR J 1825-0935 [22], the exponent for the power-law glitch-size PDF is $\simeq 0.36$, nearly the same as our calculated exponent. In many pulsars, including PSR J 1825-0935, the waiting-time PDF has an exponential tail; this is in agreement with our result [22].

We have shown that uniformly rotating vortex-containing gravitationally-bound solutions of the GPPE can be generated by starting the evolution from initial data obtained by integrating to convergence the (imaginary-time) ARGLPE (7). We have built on this GPPE and introduced a minimal model, with a single, angular, dynamical variable for a solid crust coupled with a rotating GPPE star. We have demonstrated that this model exhibits stick-slip dynamics, whose statistical properties we have characterized by computing the event-size and event-duration CPDFs $Q(\Delta J_c/J_{c_0})$ and

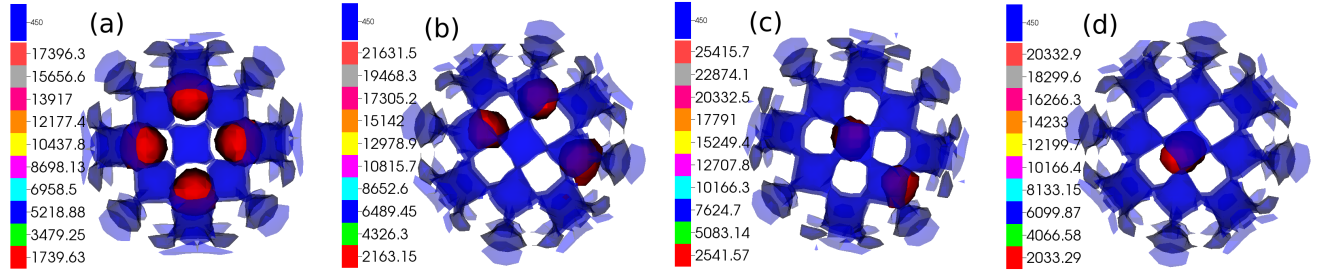


FIG. 3: Plots of crust-potential isosurfaces in blue, with $V_\theta = 450$, and of ten-level isosurfaces of $(\nabla \times (\rho v))^2$, from our DNS of the GPPE, for the representative parameter values $V_0 = 180$, $n_{\text{crust}} = 12$, $I_c = 0.01$, $r_{\text{crust}} = 1.0$, $\Delta r_{\text{crust}} = 0.15$, $\Omega_0 = 14$, and $\alpha = 0.007$ (as in Fig. 4 below) at times (a) $t = 0.06$, (b) $t = 6.48$, (c) $t = 7.38$, and (d) $t = 9.72$. For the spatiotemporal evolution of these isosurfaces see the video S2 in the Supplemental Material [28].

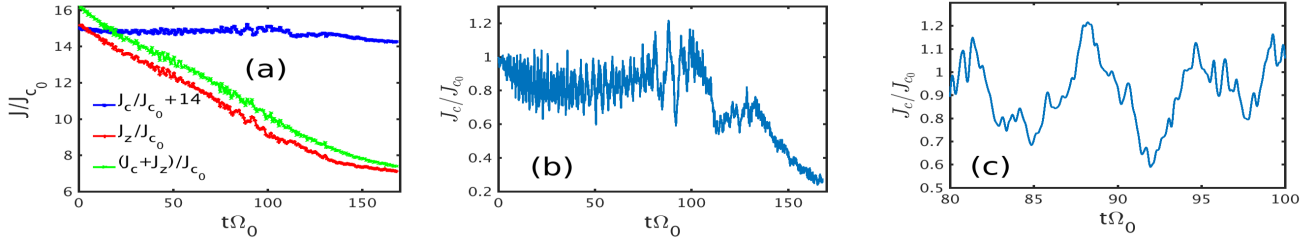


FIG. 4: (a) Plots, versus the scaled time $t\Omega_0$, of $(J_c/J_{c_0} + 14)$ [blue curve], J_z/J_{c_0} [red curve], and $(J_c + J_z)/J_{c_0}$ [green curve], where J_{c_0} is the initial angular momentum of the crust, for the representative parameter values given in Fig. 3 above. Expanded plots of J_c/J_{c_0} for (b) $0 < t\Omega_0 \lesssim 170$ and (c) $80 \leq t\Omega_0 \leq 100$.

$Q(t_{\text{ed}}\Omega_0)$, which show power-law forms, and the waiting-time CPDF $Q(t_{\text{wt}}\Omega_0)$, which exhibits an exponential tail. These SOC-type desiderata are in consonance with measurements on a class of pulsars [22].

We plan to study pulsar-glitch models that are more realistic than our minimal model. Examples include models with (a) a solid crust with 6 degrees of freedom, 3 rotational and 3 translational, instead of only one angle of rotation, or (b) a superconducting component with magnetic flux tubes. We expect that such generalizations of our minimal model should help us to understand all the types of statistical properties that are displayed by pulsar glitches in different pulsars [21–24, 30–32].

We thank DST (IN), CSIR (IN), and the Indo-French Center for Applied Mathematics (IFCAM) for their support and SERC (IISc) for computational resources.

* Electronic address: akhilesh@iisc.ac.in

† Electronic address: rahul@iisc.ac.in; also at Jawaharlal Nehru Centre For Advanced Scientific Research, Jakkur, Bangalore, India.

‡ Electronic address: brachet@phys.ens.fr

- [1] B. Haskell and A. Melatos, *International Journal of Modern Physics D* **24**, 1530008 (2015).
 [2] A. Basu *et al.*, *The Astrophysical Journal* **866**, 94 (2018).
 [3] V. Radhakrishnan and R. Manchester, *Nature* **222**, 228

(1969).

- [4] P. Boynton, E. Groth III, R. B. Partridge, and D. T. Wilkinson, *The Astrophysical Journal* **157**, L197 (1969).
 [5] R. N. Manchester, *Proceedings of the International Astronomical Union* **13**, 197 (2017).
 [6] M. Ruderman, *Nature* **223**, 597 (1969).
 [7] G. Baym, C. Pethick, D. Pines, and M. Ruderman, *Nature* **224**, 872 (1969).
 [8] T. Sidery, A. Passamonti, and N. Andersson, *Monthly Notices of the Royal Astronomical Society* **405**, 1061 (2010).
 [9] V. Khomenko and B. Haskell, *Publications of the Astronomical Society of Australia* **35**, e020 (2018).
 [10] G. Watanabe and C. J. Pethick, *Phys. Rev. Lett.* **119**, 062701 (2017).
 [11] A. Migdal, *Nuclear Physics* **13**, 655 (1959).
 [12] L. Warszawski and A. Melatos, *Monthly Notices of the Royal Astronomical Society* **415**, 1611 (2011).
 [13] L. Warszawski, A. Melatos, and N. G. Berloff, *Phys. Rev. B* **85**, 104503 (2012).
 [14] P.-H. Chavanis, *Phys. Rev. D* **84**, 043531 (2011).
 [15] P.-H. Chavanis and L. Delfini, *Phys. Rev. D* **84**, 043532 (2011).
 [16] A. K. Verma, R. Pandit, and M. E. Brachet, arXiv:1912.10172 [cond-mat.quant-gas] (2019).
 [17] P. Bak, C. Tang, and K. Wiesenfeld, *Physical review letters* **59**, 381 (1987).
 [18] J. M. Carlson and J.S. Langer, *Physical Review Letters* **62**, 2632 (1989).
 [19] H. J. Jensen, *Self-organized criticality: emergent complex behavior in physical and biological systems* (Cambridge university press, ADDRESS, 1998), Vol. 10.

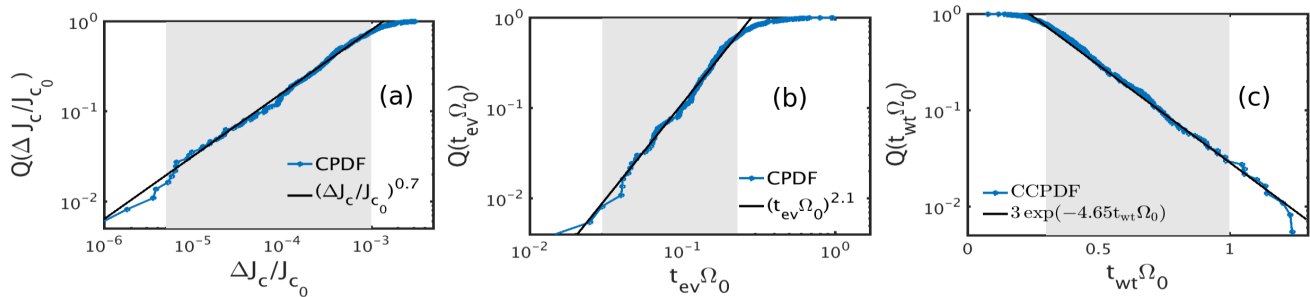


FIG. 5: Log-log (base 10) plots of: (a) the CPDF $Q(\Delta J_c/J_{c_0})$ of the event size; and (b) the CPDF $Q(t_{\text{ev}}\Omega_0)$ of the event duration. (c) Semi-log (base 10) plot of the CPDF $Q(t_{\text{wt}}\Omega_0)$. J_{c_0} and Ω_0 are, respectively, the initial angular momentum and angular velocity of the crust. Our DNS data are shown in blue; the black lines show fits (power-law or exponential) to these data in the shaded gray regions in the plots.

- [20] D. L. Turcotte, Reports on progress in physics **62**, 1377 (1999).
- [21] P. Morley and R. Garcia-Pelayo, EPL (Europhysics Letters) **23**, 185 (1993).
- [22] A. Melatos, C. Peralta, and J. Wyithe, The Astrophysical Journal **672**, 1103 (2008).
- [23] M. J. Aschwanden, Open Aca (2013).
- [24] M. J. Aschwanden *et al.*, Space Science Reviews **198**, 47 (2016).
- [25] G. Krstulovic and M. Brachet, Phys. Rev. E **83**, 066311 (2011).
- [26] V. Shukla, M. Brachet, and R. Pandit, New J. Phys. **15**, 113025 (2013).
- [27] D. Gottlieb and S. A. Orszag, *Numerical Analysis of Spectral Methods* (SIAM, Philadelphia, 1977).
- [28] Supplemental Material (2020).
- [29] J. Eby, M. Leembruggen, L. Street, P. Suranyi, and L.C.R. Wijewardhana, Phys. Rev. D **98**, 123013 (2018).
- [30] C. M. Espinoza, A. G. Lyne, B. W. Stappers, and M. Kramer, Monthly Notices of the Royal Astronomical Society **414**, 1679 (2011).
- [31] J. B. Carlin and A. Melatos, Monthly Notices of the Royal Astronomical Society **483**, 4742 (2019).
- [32] I. O. Eya, J. O. Urama, and A. E. Chukwude, Research in Astronomy and Astrophysics **19**, 089 (2019).
- [33] P. J. E. Peebles, *The large-scale structure of the universe*, 2011 ed. (Princeton University Press, Princeton, NJ, 1980).
- [34] M. Falco, S. H. Hansen, R. Wojtak, and G. A. Mamon, Monthly Notices of the Royal Astronomical Society: Letters **431**, L6 (2013).
- [35] M. K.-H. Kiessling, Advances in Applied Mathematics **31**, 132 (2003).
- [36] V. Shukla, M. Brachet, and R. Pandit, Phys. Rev. A **94**, 041602(R) (2016).
- [37] E. J. M. Madarassy and V. T. Toth, Phys. Rev. D **91**, 044041 (2015).
- [38] Note that the subtraction of the mean density on the right-hand side (RHS) of the Poisson equation 2 can be justified either by taking into account the cosmological expansion [33, 34] or by defining a Newtonian cosmological constant [35].
- [39] The first term on the RHS of Eq. (3) can be obtained from the GPPE Lagrangian augmented with the crust rotational energy $\frac{I_c}{2}(\frac{d\theta}{dt})^2$; the variation of this Lagrangian

with respect to $\bar{\psi}$ yields Eq. (1); and the variation with respect to θ yields the first term on the RHS. of Eq. (3) (see Ref. [36] for a similar procedure involving active particles in the Gross-Pitaevskii equation with Newtonian particles).

[40] For example, such states were not obtained in Ref. [37], probably because pure GPPE evolution was used, without the benefit of ARGLPE-based minimization.

[41] We have noted above that, because we use 2π -periodic coordinates to define J_z , the conservation of angular momentum is only approximate, *even if* $\alpha = 0$; also, in neutron stars, the crust angular momentum is only a few percent of the total angular momentum [2].

Supplemental Materials: Rotating self-gravitating Bose-Einstein condensates with a crust: a minimal model for pulsar glitches

In this Supplemental Material we provide details of our direct numerical simulation and some videos from our DNSs of the advective real Ginzburg-Landau-Poisson equation (ARGLPE) and the Gross-Pitaevskii-Poisson equation (GPPE) with a crust potential.

Our DNS

We solve the GPPE Eq.(1) and (2) of the main text by using a 3D Fourier pseudospectral method [S1–S3], with $\psi(x) = \sum_{|\mathbf{k}| < k_{\max}} \hat{\psi}_{\mathbf{k}} \exp(i\mathbf{k} \cdot \mathbf{x})$ and $k_{\max} = [\mathcal{N}/3]$, where \mathcal{N} is the resolution and $[\cdot]$ denotes the integer part. In the absence of the crust potential, friction, and of rotation, we obtain the conventional GPPE [see Ref. [S4], where we describe the large-scale gravitational Jeans instability. In all 3 spatial directions, our DNS uses 2π -periodic boundary conditions (PBCs), which we also use to define J_z and V_θ ; so, even if $\alpha = 0$, the conservation of the total angular momentum holds only approximately, for the system does not have rotational invariance in \mathbb{R}^3 .

We use the units that we have employed in Ref. [S4], where we have shown that non-rotating, compact, gravitationally bound objects have a radius of gyration, $R_G = \sqrt{\frac{\int_V \rho(r)r^2 d\mathbf{r}}{\int_V \rho(r) d\mathbf{r}}}$ that is of the order of the length scale $R_a = \sqrt{\frac{a\hbar^2}{G_N m^3}} = \sqrt{\frac{g}{G}}$. Our DNS employs a $(2\pi)^3$ periodic computational box, so we normalize ψ such that $N = N_0 = (2\pi)^3$; and, in DNS time and length units, $\hbar = 1$ and $m = 1$. For time marching we use the fourth-order Runge-Kutta scheme.

Videos from our DNSs

- The spatiotemporal evolution of $|\psi(\mathbf{x}, t)|^2$ from our ARGLPE study, for $\mathcal{N} = 256$, $G = 800$ $g = 80$, and $\Omega = 60$ (cf., Fig. 2 in the main paper) is given in the video V1.
- The spatiotemporal evolution of the crust-potential isosurfaces in blue, with $V_\theta = 450$, and isosurfaces of $(\nabla \times (\rho v))^2$, from our DNS of the GPPE, for the representative parameter values $V_0 = 180$, $n_{\text{crust}} = 12$, $I_c = 0.01$, $r_{\text{crust}} = 1.0$, $\Delta r_c = 0.15$, $\Omega_0 = 14$, and $\alpha = 0.007$ (cf., Fig. 3 in the main paper) is given in the video V2.

* Electronic address: akhilesh@iisc.ac.in

† Electronic address: rahul@iisc.ac.in;

also at Jawaharlal Nehru Centre For Advanced Scientific Research, Jakkur, Bangalore, India.

‡ Electronic address: brachet@phys.ens.fr

[S1] G. Krstulovic and M. Brachet, Phys. Rev. E **83**, 066311 (2011).

[S2] V. Shukla, M. Brachet, and R. Pandit, New J. Phys. **15**, 113025 (2013).

[S3] D. Gottlieb and S. A. Orszag, *Numerical Analysis of Spectral Methods* (SIAM, Philadelphia, 1977).

[S4] A. K. Verma, R. Pandit, and M. E. Brachet, arXiv:1912.10172 [cond-mat.quant-gas] (2019).